

Carbon-oxygen-neon mass nuclei in superstrong magnetic fields

Martin Stein,^{*} Joachim Maruhn,[†] and Armen Sedrakian[‡]

Institute for Theoretical Physics, J. W. Goethe-University, D-60438 Frankfurt am Main, Germany

P.-G. Reinhard[§]

Institut für Theoretische Physik, Universität Erlangen, D-91054 Erlangen, Germany

(Dated: March 1, 2022)

The properties of ^{12}C , ^{16}O , and ^{20}Ne nuclei in strong magnetic fields $B \simeq 10^{17}$ G are studied in the context of strongly magnetized neutron stars and white dwarfs. The SKY3D code is extended to incorporate the interaction of nucleons with the magnetic field and is utilized to solve the time-independent Hartree-Fock equations with a Skyrme interaction on a Cartesian three-dimensional grid. The numerical solutions demonstrate a number of phenomena, which include a splitting of the energy levels of spin-up and -down nucleons, spontaneous rearrangement of energy levels in ^{16}O at a critical field, which leads to jump-like increases of magnetization and proton current in this nucleus, and evolution of the intrinsically deformed ^{20}Ne nucleus towards a more spherical shape under increasing field strength. Many of the numerical features can be understood within a simple analytical model based on the occupation by the nucleons of the lowest states of the harmonic oscillator in a magnetic field.

I. INTRODUCTION

The studies of nuclei and bulk nuclear matter in strong magnetic fields are motivated by the astrophysics of strongly magnetized neutron stars (magnetars) and white dwarfs. The surface fields of magnetars have been inferred to be from observations in the range of 10^{15} G. The interior fields of magnetars can be several orders of magnitude larger than their surface fields [1].

The electromagnetic energy of the interaction of baryons with the B field becomes of the order of the nuclear scale \sim MeV for fields $10^{16} - 10^{17}$ G and can arise from current-field (for electrically charged particles) and spin-field (for charge neutral particle) interaction. Such interaction can affect the properties of nuclei, including their shell structure, binding energies, and rms radii. This, in turn, can affect the structure and composition of the interiors of neutron stars and white dwarfs where nuclei are predicted to exist, as well as the transport and weak interaction (neutrino emission and absorption) processes due to the changes in charged particle dynamics and transition matrix elements.

The equation of state and composition of inhomogeneous nuclear matter featuring nuclei in strong magnetic fields have been studied using various methods including modification of the Thomas-Fermi model [2], liquid drop model [3], nuclear shell Nilsson model [4, 5], relativistic density functional theory [6, 7], and non-relativistic Skyrme functional theory [8]. It has been shown that bulk properties of nuclei and shell structure as well as their shape can be significantly affected if the magnetic

field is of the order of 10^{17} G and larger. These studies were carried out in the context of neutron star crusts and have concentrated on heavy nuclei beyond (and including) ^{56}Fe .

In this work we consider the properties of carbon-oxygen-neon mass nuclei in strong magnetic fields. Our motivation for doing so is threefold. Firstly, some isolated neutron stars are known to have atmospheres composed of ^{12}C , as is well established in the case of the compact object in Cas A [9]. Carbon plays also an important role in the physics of accreting neutron stars, for example, in the superbursts which are associated by unstable ignition of carbon at depth characterized by the density $\rho \simeq 10^9$ g cm $^{-3}$ [10]. Apart from ^{12}C , there are also substantial fractions of oxygen and neon mass nuclei produced in the crusts of accreting neutron stars through nuclear reaction networks (Ref. [10] Table I and Figs. 4 and 5). The composition of the surfaces of magnetars and their properties under accretion are not known. However, one can anticipate the role played by these nuclei in the physics of magnetars, by extrapolating from the physics of low-field neutron stars. Secondly, white dwarfs models composed of ^{12}C , ^{16}O , or ^{20}Ne are standard in the physics of these compact objects in the non-magnetized regime. The superluminous type-I supernovae were suggested recently to originate from supermassive strongly magnetized white dwarfs [11] with magnetic fields in the range 10^{17} G. If such objects exist (for a discussion see [12]) they would provide the environment where light nuclei would be subjected to intense B fields. Thirdly, besides the astrophysical motivation, there is a technical aspect to our study, as it is a first attempt to include magnetic fields in the widely used SKY3D code [13]. Therefore, another motivation of our study is to provide a benchmark for future studies that will include magnetic fields on simple enough systems that are easily tractable, and ^{12}C , ^{16}O , or ^{20}Ne nuclei are optimal in this respect. As we show below, the splitting of the levels induced by the

^{*}mstein@th.physik.uni-frankfurt.de

[†]maruhn@th.physik.uni-frankfurt.de

[‡]sedrakian@th.physik.uni-frankfurt.de

[§]paul-gerhard.reinhard@physik.uni-erlangen.de

B field in these nuclei can be easily understood on the basis of a harmonic oscillator model; because of the small number of levels the comparison between the numerical and analytical results becomes possible. (Indeed, in heavy nuclei the number of levels can become very large, which would make such comparison impractical).

The density-functional-based Hartree-Fock (HF) theory provides an accurate and flexible framework to study a variety of low-energy nuclear phenomena. The public domain SKY3D code [13], solves the HF equations on a 3D grid (i.e. without any assumptions about the underlying symmetries of the nuclei) and is based on the Skyrme density functional. It has already been utilized to study a broad range of problems ranging from low-energy heavy-ion collisions to nuclear structure to exotic shapes in crusts of neutron stars (for references see Ref. [13]).

In this work we report on the first implementation of a strong magnetic field in the SKY3D code via extension of the Hamiltonian (and the associated density functional) to include all relevant terms reflecting the interaction of the magnetic field with nucleons. We concentrate on the static solutions, which requires the solution of time-independent Hartree-Fock equations. As an initial application we report convergent studies of the carbon-oxygen-neon mass range nuclei in strong fields.

This paper is organized as follows. In Sec. II we describe briefly the underlying theory and the modifications to the numerical code needed to include B fields. We present our results in Sec. III where we first set up a simple analytical model which is then compared with numerical results. A number of observables such as energy levels, spin- and current-densities, as well as deformations are discussed. Our conclusions are summarized in Sec. IV.

II. THEORY AND NUMERICAL CODE

A. Theory

We consider a nucleus in a magnetic field which is described by the Hamilton operator $\hat{h}_q = \hat{h}_q^{(0)} + \hat{h}_q^{(B)}$, where $q \in \{p, n\}$ specifies the isospin of a nucleon and $\hat{h}_q^{(0)}$ is the Hamiltonian in the absence of a B field, which is given by Eq. (8) of Ref. [13]. It is constructed in terms of densities and currents of nucleons. The term $\hat{h}_q^{(B)}$ which is due to the B field is given by

$$\hat{h}_q^{(B)} = - \left(\mathbf{l} \delta_{q,p} + g_q \frac{\boldsymbol{\sigma}}{2} \right) \cdot \tilde{\mathbf{B}}_q, \quad (1)$$

where $\tilde{\mathbf{B}}_q \equiv (e\hbar/2m_qc)\mathbf{B}$, $\boldsymbol{\sigma}$ is the spin Pauli matrix, and \mathbf{l} is the (dimensionless) orbital angular momentum. These are related to the spin \mathbf{S} and the orbital angular momentum \mathbf{L} via $\mathbf{S} = \hbar\boldsymbol{\sigma}/2$ and $\mathbf{L} = \hbar\mathbf{l}$, where $g_n = -3.826$ and $g_p = 5.585$ are the g factors of neutrons and protons. The Kronecker-delta takes into account the fact that neutrons do not couple with their orbital angular momenta.

Starting from the Hamiltonian \hat{h}_q one can construct the density functional (DF) in the basis Hartree-Fock wave functions. We use the DF which contains the kinetic energy, the nuclear Skyrme interaction, the Coulomb energy, and the correlation correction to the mean-field DF. In principle the pairing correction can be added to the DF, but we ignore it here because of its overall smallness and because the S -wave pairing would be quenched by the magnetic field [14]. The correlation correction in the DF includes those corrections which reflect the beyond-mean-field contributions.

B. Numerical code and procedure

We have used the code SKY3D to find iteratively the solution of the static HF equation in strong magnetic fields. The equations are solved using successive approximations to the wave functions on a three-dimensional Cartesian grid, which has 32 points along each direction and a distance between the points of 1.0 fm. (We varied the parameters of the mesh within reasonable values and made sure that the physical results are unchanged). To accelerate the iteration a damping of the kinetic term is performed. The following ranges of the two numerical parameters of the damped gradient step have been used - the step size $\delta = 0.4$ and the damping regulator $E_0 = 100$ MeV. After performing a wave-function iteration steps, the densities of the nucleons are updated and new mean fields are computed. This provides the starting point for the next iteration. The iterations are continued until convergence to the desired accuracy is achieved. As a convergence criterion the average energy variance or the fluctuation of single-particle states is used. To initialize the problem we use harmonic oscillator states and include an unoccupied nucleon state. The radii of the harmonic oscillator states are $r_{\text{h.o.}} \simeq 3$ fm. Our computations were carried out with the SV-bas version of the Skyrme force [15]. The magnetic field direction was chosen along the z direction, but other directions were also tested to produce identical results. Initially nuclei with $B = 0$ were computed, thereafter the magnetic field was incremented with steps of about $0.25\sqrt{\text{MeV fm}^{-3}}$ as long as the convergence was achieved for the number of iterations $N_i \leq 4000$. The direction of the B field was chosen always as the z axis of Cartesian coordinates, unless stated otherwise.

To access the shape and size of the nuclei we examined the radii r_{rms} , the total deformation β and the triaxiality γ (for definitions see, e. g., [16]). Here $\gamma = 0^\circ$ refers to a prolate deformed nucleus, $\gamma = 60^\circ$ refers to an oblate deformed nucleus, and angles between $\gamma = 0^\circ$ and $\gamma = 60^\circ$ refer to a deformation in a state between prolate and oblate. If $\beta = 0$ the nucleus is spherical (undeformed) independent of γ . For non-zero β , the nuclei are deformed.

III. RESULTS

In this work we report the studies of symmetrical nuclei ^{12}C , ^{16}O , and ^{20}Ne in a strong magnetic field, for which we evaluated the energy levels of neutrons and protons, their spin and current densities, as well as deformation parameters. Below we show selected results from these studies, which highlight the physics of nuclei in strong B fields.

A. Analytical estimates

Before discussing the numerical results we provide approximate analytical formulas for energy level splitting and z components of angular momentum and spin in terms of Clebsch-Gordan coefficients. We adopt the definition of the Clebsch-Gordan coefficients [16]:

$$|JMls\rangle = \sum_{m_l m_s} |lm_l sm_s\rangle (lsJ|m_l m_s M), \quad (2)$$

where l is the orbital angular momentum, s the spin, and J the total angular momentum and m_l , m_s , and M are the z components of l , s , and J , respectively. The following conditions need to be fulfilled:

$$m_l + m_s = M, \quad (3a)$$

$$|l - s| \leq J \leq l + s. \quad (3b)$$

For nucleons $s = 1/2$ always and, therefore, $m_s = \pm 1/2$, l is a non-negative integer number, and m_l is an integer number, which can be positive, negative, or zero. Thus, J assumes non-negative half-integer numbers; M assumes half-integer numbers, which can be positive or negative. Writing out formula (2) for the lowest states of a nucleus and inserting the values of the Clebsch-Gordan coefficients we find for the s states

$$s_{1/2}(M = -\frac{1}{2}) : \quad |\frac{1}{2}, -\frac{1}{2}, 0\rangle = |0, +0, -\frac{1}{2}\rangle, \quad (4a)$$

$$s_{1/2}(M = +\frac{1}{2}) : \quad |\frac{1}{2}, +\frac{1}{2}, 0\rangle = |0, +0, \frac{1}{2}\rangle, \quad (4b)$$

where on both side of these equations we omitted the trivial value of spin $s = 1/2$ appearing in Eq. (2). For

the p states we find

$$p_{3/2}(M = -\frac{3}{2}) : \quad (5a)$$

$$|\frac{3}{2}, -\frac{3}{2}, 1\rangle = |1, -1, -\frac{1}{2}\rangle, \quad (5b)$$

$$p_{3/2}(M = -\frac{1}{2}) : \quad (5c)$$

$$|\frac{3}{2}, -\frac{1}{2}, 1\rangle = \frac{1}{\sqrt{3}} |1, -1, \frac{1}{2}\rangle + \sqrt{\frac{2}{3}} |1, +0, -\frac{1}{2}\rangle,$$

$$p_{3/2}(M = +\frac{1}{2}) : \quad (5c)$$

$$|\frac{3}{2}, +\frac{1}{2}, 1\rangle = \sqrt{\frac{2}{3}} |1, +0, \frac{1}{2}\rangle + \frac{1}{\sqrt{3}} |1, +1, -\frac{1}{2}\rangle,$$

$$p_{3/2}(M = +\frac{3}{2}) : \quad (5d)$$

$$|\frac{3}{2}, +\frac{3}{2}, 1\rangle = |1, +1, \frac{1}{2}\rangle, \quad (5e)$$

$$p_{1/2}(M = -\frac{1}{2}) : \quad (5e)$$

$$|\frac{1}{2}, -\frac{1}{2}, 1\rangle = -\sqrt{\frac{2}{3}} |1, -1, \frac{1}{2}\rangle + \frac{1}{\sqrt{3}} |1, +0, -\frac{1}{2}\rangle,$$

$$p_{1/2}(M = +\frac{1}{2}) : \quad (5f)$$

$$|\frac{1}{2}, +\frac{1}{2}, 1\rangle = -\frac{1}{\sqrt{3}} |1, +0, \frac{1}{2}\rangle + \sqrt{\frac{2}{3}} |1, +1, -\frac{1}{2}\rangle.$$

The states can be divided into mixed states that are linear combinations of certain $|lm_l sm_s\rangle$ states and pure states which involve only one set of these quantum numbers. The energy levels of spin-up and -down particles are split in a magnetic field. This splitting is given by

$$\Delta E_q(J, M, l) = \langle J, M, l | \hat{h}_q^{(B)} | J, M, l \rangle, \quad (6)$$

which can be expressed in terms of the Clebsch-Gordan coefficients

$$\Delta E_q(J, M, l) = - \sum_{m_l, m_s} (l, J | m_l, m_s, M)^2 \tilde{B}_q \times (m_l \delta_{q,p} + g_q m_s). \quad (7)$$

The z -components of the angular momentum and spin can be as well expressed through the Clebsch-Gordan coefficients according to

$$\langle S_z(J, M, l) \rangle = \hbar \sum_{m_l, m_s} m_s (l, J | m_l, m_s, M)^2, \quad (8)$$

$$\langle L_z(J, M, l) \rangle = \hbar \sum_{m_l, m_s} m_l (l, J | m_l, m_s, M)^2. \quad (9)$$

Table I lists values of energy splitting, and z components of angular momentum and spin according to Eqs. (7)-(9) for neutron and proton states. These analytical results can be compared to the results of the SKY3D code, to which we now turn.

B. Energy levels

The states of protons and neutrons in ^{16}O nucleus are shown in Figs. 1 and 2 as a function of the magnetic field. For the fields $B \geq 10^{16}$ G the split in the energy levels of spin-up and spin-down states becomes sizable (of

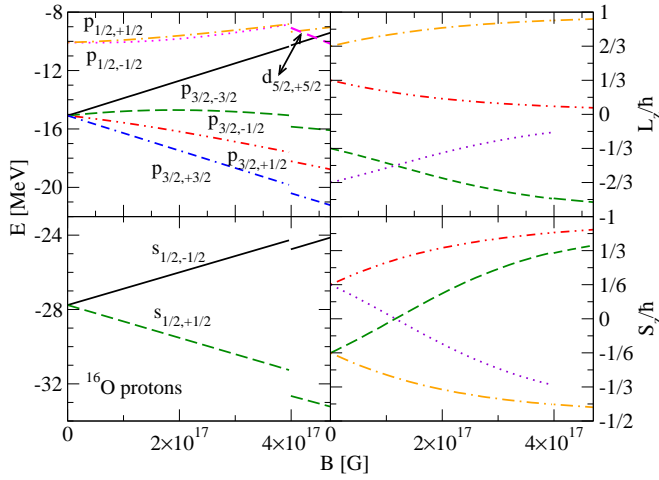


FIG. 1: Dependence of proton energy levels of ^{16}O on magnetic field (left panels) and the projections of the angular momentum and spin on the z axis. The lower panels show the s -states, the upper ones the p states and a d state for large B fields. A rearrangement of the energy levels is seen in the upper left panel at the magnetic field $B \geq 4 \times 10^{17}$ G. This is related to the rearrangement of the proton levels as discussed in the text.

TABLE I: Energy splitting and z components of angular momentum and spin for the s and p states. The values of quantities for negative M differ from the corresponding ones for positive M by overall sign and are not shown.

	$s_{1/2}(M = \frac{1}{2})$	$p_{3/2}(M = \frac{1}{2})$	$p_{3/2}(M = \frac{3}{2})$	$p_{1/2}(M = \frac{1}{2})$
$\frac{\Delta E_n}{g_n B_n}$	$-\frac{1}{2}$	$-\frac{1}{6}$	$-\frac{1}{2}$	$\frac{1}{6}$
$\frac{\Delta E_p}{g_p B_p}$	$-\frac{1}{2}$	$-\frac{1}{3}(g_p^{-1} + \frac{1}{2})$	$-(g_p^{-1} + \frac{1}{2})$	$-\frac{2}{3}(g_p^{-1} - \frac{1}{2})$
$\langle L_z \rangle / \hbar$	0	$\frac{1}{3}$	1	$\frac{2}{3}$
$\langle S_z \rangle / \hbar$	$\frac{1}{2}$	$\frac{1}{6}$	$\frac{1}{2}$	$-\frac{1}{6}$

the order of the nuclear scale MeV). For the s states the splitting increases linearly with the magnitude of magnetic field. For p states this dependence is more complicated. Below the critical field $B_c[^{16}\text{O}] = 4.0 \times 10^{17}$ G, the filling of the states corresponds to that of the lowest available states of the harmonic oscillator. However, for fields larger than $B_c[^{16}\text{O}]$ the occupation pattern for protons changes: the $d_{5/2}, M = +5/2$ state becomes occupied instead of the $p_{1/2}, M = -1/2$ state (which is not shown above this field value) in Fig. 1. We also find that above the critical field $B_c[^{16}\text{O}]$ the energy levels undergo an abrupt rearrangement. For the pure states (all s states and p states with $M = \pm 3/2$), we obtain a good agreement between the numerical and analytical results for the

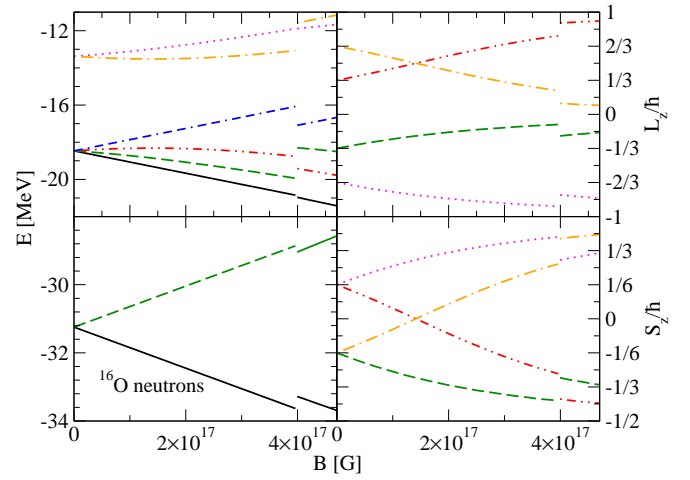


FIG. 2: Same as Fig. 1, but for neutrons.

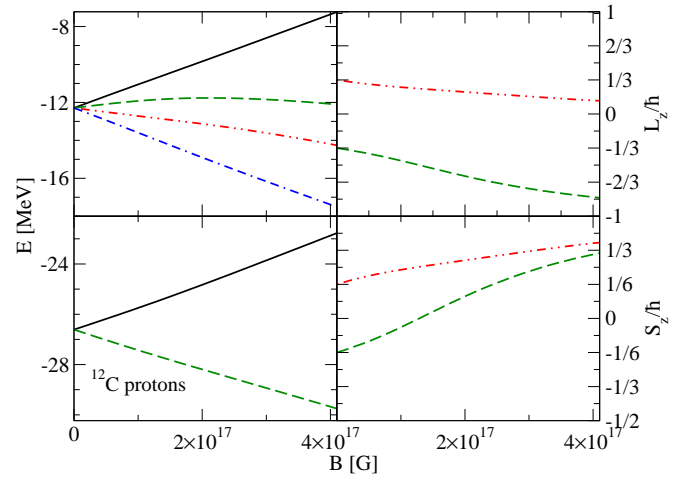


FIG. 3: Same as Fig. 1, but for protons in ^{12}C . No rearrangement of levels is observed for this nucleus.

energy levels. For the mixed states the discrepancy between the numerical and analytical results is below 10% of the energy of the corresponding level. The computations of the energy levels for the ^{12}C nucleus show the same basic features seen already in the case of ^{16}O , see Figs. 3 and 4. In this case the numerical and analytical differ by at most 10% of the energy of the levels, the discrepancy increasing with the field. The same applies to the case of the ^{20}Ne nucleus, but classification of the levels in this case is more complex because apart from the

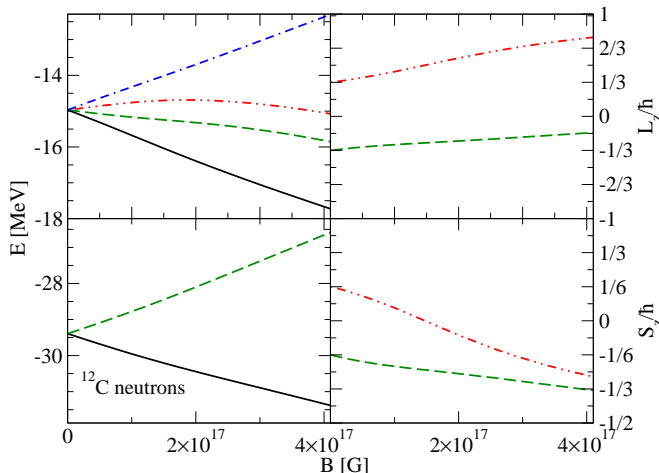


FIG. 4: Same as Fig. 3, but for neutrons.

$1s$ and $1p$ states two $1d_{5/2}$ states should be filled. This nucleus is deformed in the ground state and the axis of the deformation may not coincide with the direction of the magnetic field, in which case there are no states with half-integer values of $(\langle L_z \rangle + \langle S_z \rangle)/\hbar$. In addition to the energy levels, we have also computed the z components of orbital angular momentum $\langle L_z \rangle$ and spin $\langle S_z \rangle$ of neutrons and protons as functions of the magnetic field. The results are shown in Figs. 1 and 2. For the s states, defined in Eqs. (4a) and (4b), as well as pure p states (5a) and (5d) we obtain integer or half integer numbers for $\langle L_z \rangle/\hbar$ or $\langle S_z \rangle/\hbar$ which are identical to the quantum numbers m_l or m_s , respectively, are independent of the magnetic field, and therefore are not shown in Figs. 1 and 2.

For mixed states given by Eqs. (5b), (5c), (5e) and (5f), $\langle L_z \rangle$ and $\langle S_z \rangle$ change as functions of the magnetic field as seen from these figures. For these states at any magnetic field $M = m_l + m_s = (\langle L_z \rangle + \langle S_z \rangle)/\hbar$ is a good quantum number. In the limit of weak magnetic fields the angular momentum and spin are coupled via the l - s coupling. Then $\langle L_z \rangle$ and $\langle S_z \rangle$ for each state are given according to Table I. Because of the l - s coupling the vectors of \mathbf{L} and \mathbf{S} are not aligned with the magnetic field separately. The influence of the weak magnetic field on the system is described by the Zeeman effect. In the regime of strong magnetic fields the l - s coupling is ineffective, i.e., the orbital angular momentum l and the spin s couple separately to the magnetic field. In this case, the mixed states reach asymptotically the following non

mixed states:

$$p_{3/2}(M = -\frac{1}{2}) : \quad |1, +0, -\frac{1}{2}\rangle, \quad (10a)$$

$$p_{3/2}(M = +\frac{1}{2}) : \quad |1, +1, -\frac{1}{2}\rangle, \quad (10b)$$

$$p_{1/2}(M = -\frac{1}{2}) : \quad |1, -1, \frac{1}{2}\rangle, \quad (10c)$$

$$p_{1/2}(M = +\frac{1}{2}) : \quad |1, +0, \frac{1}{2}\rangle. \quad (10d)$$

Thus we observe a smooth transition from the l - s to the separate l - B and s - B coupling as the magnetic field is increased, which can be viewed as a transition from the Zeeman to the Paschen-Back effect. Finally we note that for the $d_{5/2}(M = +5/2)$ state $\langle L_z \rangle/\hbar = m_l = 2$ and $\langle S_z \rangle/\hbar = m_s = 1/2$ assume constant values for all magnetic fields and are therefore not shown in Fig. 1. The key features observed for components $\langle L_z \rangle$ and $\langle S_z \rangle$ of ^{16}O persist in the case of ^{12}C and we do not show them here.

C. Spin and current densities

We have extracted the current and spin densities as a functions of the magnetic field for the ^{12}C , ^{16}O , and ^{20}Ne nuclei. It is more convenient to show the collective flow velocity instead of the currents by dividing these with the particle density. The velocity distribution in ^{16}O is shown in Fig. 5. The top and middle panels compare the velocity distribution for neutrons and protons for the field $B = 3.9 \times 10^{17}$ G; the background shows the density distribution within the nucleus. It is seen that the magnitude of the proton current is by a factor of 4 larger than the neutron current. We also observe that the proton and neutron currents are counter-moving and concentrated around the surface of the nucleus. Note that the current density is shown in the plane orthogonal to the field. In the case of ^{12}C we find current patterns of neutrons and protons similar to those seen in ^{16}O . The currents are counter-moving for neutrons and protons, their magnitudes increase with the field value and are mostly concentrated at the surface of the nuclei. Because there is no rearrangement seen for ^{12}C this increase, in contrast to ^{16}O , is gradual. The velocities of protons in ^{20}Ne are shown in Fig. 6 for two magnetic fields $B = 4.0 \times 10^{13}$ G and the maximal studied field $B = 4.9 \times 10^{17}$ G. The four orders of magnitude increase in the field leads to an increase in the maximal current by about the same factor. The current is concentrated at the surface of the field; note that the magnetic field induces a change in the shape of the nucleus (density distribution) which in turn affects the pattern of currents, which are more circular for a larger magnetic field.

We consider now the spin density of neutrons and protons in the nuclei under consideration and the effect of the spin interaction with the magnetic field. The spin-density for ^{16}O is shown in Fig. 7. The spins of neutrons and protons are anti-parallel as expected from Eq. (1). In the case of ^{16}O the spin polarization increases abruptly for protons because of the rearrangement of the levels.

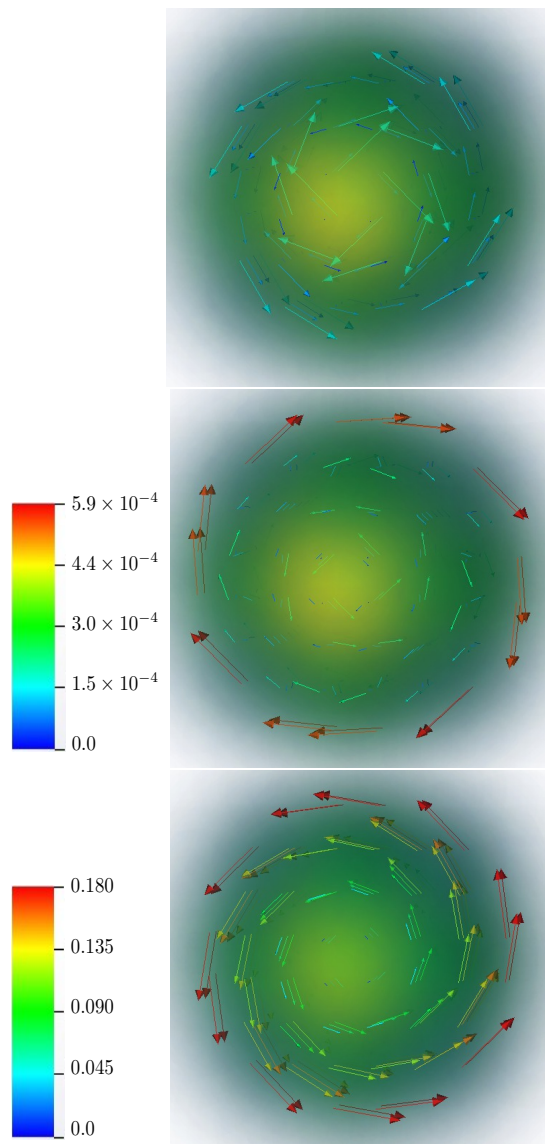


FIG. 5: Velocity distribution for neutrons (upper panel) and protons (middle and bottom panels) in ^{16}O . The upper and middle panels have the same color coding show on the left and correspond to magnetic field $B = 3.9 \times 10^{17}$ G. The bottom panel with its color coding corresponds to magnetic field $B = 4.1 \times 10^{17}$ G $> B_c[^{16}\text{O}]$. The background shows the density distribution with maximum 0.155 fm^{-3} at the center (yellow color) to the boundary where the density drops to zero (dark blue). The velocity is shown in units of speed of light.

For weak magnetic fields the l - s coupling is dominant therefore the alignment of the spins is not pronounced; for strong magnetic fields the spins are aligned with the z -axis. We find that in the case of ^{12}C the spin alignment is more pronounced than for ^{16}O , i.e., ^{12}C is more polarizable. In Fig. 8 we show the spin polarization in the ^{20}Ne nucleus, where the new feature is the deformation of the nucleus in the ground state in the absence of a magnetic field. For small magnetic fields a clear evidence of two symmetry axes is present. For larger magnetic fields

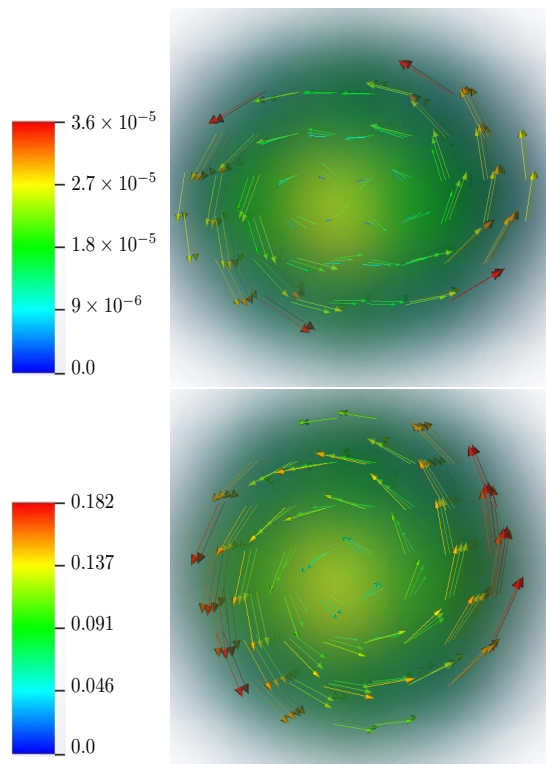


FIG. 6: Same as Fig. 5, but for protons in ^{20}Ne and for fields $B = 4.0 \times 10^{13}$ G (top panel) and $B = 4.9 \times 10^{17}$ G (bottom panel).

the spin polarization by the magnetic field directs the spin alongs the field axis (z direction). We note that in all cases protons and neutron show quantitatively similar polarization (the minor difference coming from different values of their g factors).

D. Nuclear shapes

Finally, we want to consider the shape and the size of the ^{16}O nucleus for non-zero magnetic fields. For $B < B_c[^{16}\text{O}]$, the lowest states of the harmonic oscillator are filled and the shape of the nucleus is spherical. Its radius is $r_{\text{rms}} = 2.69$ fm. For $B > B_c[^{16}\text{O}]$ the nucleus is deformed with deformation parameters $\beta = 0.1$ and $\gamma = 60^\circ$, which implies that the deformation is oblate. The mean radius is $r_{\text{rms}} = 2.72$ fm in this case. The redistribution of neutron and proton states above the critical field has the effect of slightly deforming the nucleus from its spherical shape. We stress that the redistribution is found to be abrupt and therefore the change in the shape of the nucleus is abrupt as well.

In the case of the ^{12}C nucleus we find that the shape of the nucleus does not change much with increasing magnetic field. For a zero field it is spherical symmetric with $r_{\text{rms}} = 2.47$ fm, increasing slightly to 2.51 fm for $B_c = 4.1 \times 10^{17}$ G. Increasing the magnetic field also re-

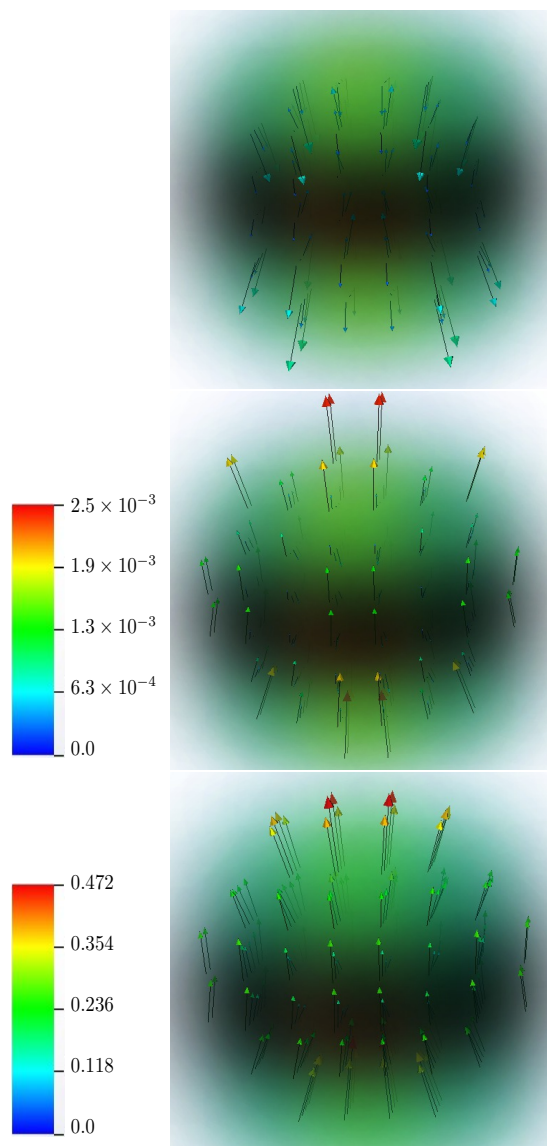


FIG. 7: The ratio of the spin density to the particle density for neutrons (upper panel) and protons (middle and bottom panel) for ^{16}O nucleus. The magnetic field z axis is directed from bottom to top. The upper and middle panel have the same color coding shown on the left and correspond to magnetic field $B = 3.9 \times 10^{17}$ G. The bottom panel with its color coding corresponds to magnetic field $B = 4.1 \times 10^{17}$ G.

sults in a smooth deformation from $\beta = 0$ at $B = 0$ to $\beta = 0.071$ for B_c . The deformation is always oblate with $\gamma = 60^\circ$.

The deformation of the ^{20}Ne nucleus with the magnetic field is continuous and in contrast to the other examples above, the nucleus is deformed for a vanishing magnetic field. We find that its radius r_{rms} slightly decreases from 2.93 fm to 2.87 fm with the magnetic field. However, the β parameter decreases from 0.32 to 0.15, i.e., to a value which is less than half of the original one. This is the only example of a continuous significant change in defor-

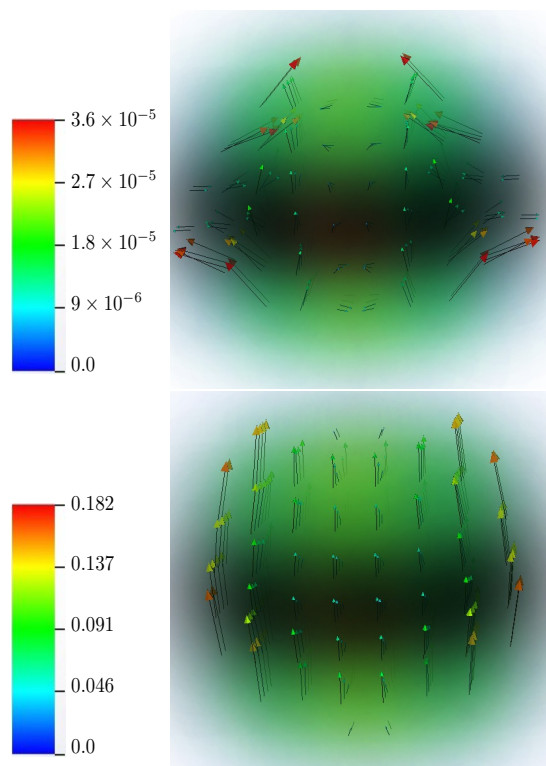


FIG. 8: Same as in Fig. 7 for protons in ^{20}Ne and for fields $B = 4.0 \times 10^{13}$ G (top panel) and $B = 4.9 \times 10^{17}$ G (bottom panel).

mation as a function of magnetic field. The parameter γ starts at 0° for $B = 0$, but increases asymptotically to 11° implying a change from a purely prolate deformed nucleus to a mainly prolate deformed one. This evolution of ^{20}Ne nucleus from deformed to the more spherical shape is visualized in Fig. 6.

IV. CONCLUSIONS

We have performed numerical computations of ^{12}C , ^{16}O , and ^{20}Ne nuclei in strong magnetic fields using an extension of the SKY3D code, which solves Hartree-Fock equations on a three-dimensional grid in a strong magnetic field. The code is based on the Skyrme density functional. Common features found for all three nuclei are (i) the splitting of energy states, which are on the order of MeV for fields $B \sim 10^{17}$ G; (ii) the increase in spin polarization along the magnetic field as the field is increased, which is characterized by a transition from a regime where l - s coupling is dominant to a regime where l and s couple directly to the magnetic field; and (iii) an increase in the flow-velocity in the plane orthogonal to the field with increasing magnetic fields. A number of features are peculiar to specific nuclei and are listed below:

- A rearrangement of energy levels in ^{16}O nucleus

is observed at a critical field 4.1×10^{17} G, which is accompanied by an abrupt increase in the magnetization of the nucleus and an increase in the velocity flow. This also leads to deformation of the nucleus from its original spherical shape at vanishing value of the field.

- The ^{12}C nucleus does not change its shape in the magnetic field and there are no energy level rearrangements as seen in ^{16}O . It is found to be more easily polarizable than the heavier nuclei.
- The ^{20}Ne nucleus is deformed in the ground state. It undergoes significant continuous change in its shape as the magnetic field is increased. The deformation is diminished by a factor of 2 for fields $B \simeq 4.1 \times 10^{17}$ G.
- We have shown that a simple analytical model which fills in the harmonic oscillator states in the magnetic field accounts well for the energy splitting of ^{12}C and ^{16}O nuclei as well as their angular momenta and spin projections. In the case of ^{20}Ne the analytical model is less reliable; it can reproduce qualitatively features obtained with the SKY3D code; however, because of the nuclear de-

formation, the magnetic field needs to be directed along the x -axis instead of the z -axis.

Phenomenologically the most important aspect of these findings is the splitting of the levels in nuclei as a function of the B field. When this splitting is on the order of the temperature it will have an important impact on all transport processes and on neutrino and photon emission and absorption, as well as on the reaction rates.

Looking ahead, we would like to extend these studies to nuclei with larger mass numbers and beyond the stability valley in the direction of neutron-rich nuclei that occur in nonaccreting neutron stars [17]. The possibility of non-spherical and extended nuclei (pasta phases [18]) can also be considered in this context.

Acknowledgments

M. S. acknowledges support from the HGS-HIRe graduate program at Frankfurt University. A. S. is supported by the Deutsche Forschungsgemeinschaft (Grant No. SE 1836/3-1) and by the NewCompStar COST Action MP1304.

-
- [1] R. Turolla, S. Zane, and A. L. Watts, Reports on Progress in Physics **78**, 116901 (2015), 1507.02924.
 - [2] I. Fushiki, E. H. Gudmundsson, and C. J. Pethick, Astrophys. J. **342**, 958 (1989).
 - [3] D. Lai and S. L. Shapiro, Astrophys. J. **383**, 745 (1991).
 - [4] V. N. Kondratyev, T. Maruyama, and S. Chiba, Physical Review Letters **84**, 1086 (2000).
 - [5] V. N. Kondratyev, T. Maruyama, and S. Chiba, Astrophys. J. **546**, 1137 (2001).
 - [6] D. Peña Arteaga, M. Grasso, E. Khan, and P. Ring, Phys. Rev. C **84**, 045806 (2011), 1107.5243.
 - [7] D. Basilico, D. P. Arteaga, X. Roca-Maza, and G. Colò, Phys. Rev. C **92**, 035802 (2015), 1505.07304.
 - [8] N. Chamel, R. L. Pavlov, L. M. Mihailov, C. J. Velchev, Z. K. Stoyanov, Y. D. Mutafchieva, M. D. Ivanovich, J. M. Pearson, and S. Goriely, Phys. Rev. C **86**, 055804 (2012), 1210.5874.
 - [9] B. Posselt, G. G. Pavlov, V. Suleimanov, and O. Kargaltsev, Astrophys. J. **779**, 186 (2013), 1311.0888.
 - [10] J. Stevens, E. F. Brown, A. Cumming, R. Cyburt, and H. Schatz, Astrophys. J. **791**, 106 (2014), 1405.3541.
 - [11] U. Das and B. Mukhopadhyay, International Journal of Modern Physics D **22**, 1342004 (2013), 1305.3987.
 - [12] N. Chamel, E. Molter, A. F. Fantina, and D. P. Arteaga, Phys. Rev. D **90**, 043002 (2014).
 - [13] J. A. Maruhn, P.-G. Reinhard, P. D. Stevenson, and A. S. Umar, Computer Physics Communications **185**, 2195 (2014), 1310.5946.
 - [14] M. Stein, A. Sedrakian, X.-G. Huang, and J. W. Clark, Phys. Rev. C **93**, 015802 (2016), 1510.06000.
 - [15] P. Klüpfel, P.-G. Reinhard, T. J. Bürvenich, and J. A. Maruhn, Phys. Rev. C **79**, 034310 (2009).
 - [16] W. Greiner and J. A. Maruhn, *Kernmodelle*, vol. 11 of *Theoretische Physik* (Verl. Harri Deutsch, Thun, Frankfurt am Main, 1995), ISBN 3-87144-977-6.
 - [17] R. N. Wolf, D. Beck, K. Blaum, C. Böhm, C. Borgmann, M. Breitenfeldt, N. Chamel, S. Goriely, F. Herfurth, M. Kowalska, et al., Phys. Rev. Lett. **110**, 041101 (2013).
 - [18] I. Sagert, G. I. Fann, F. J. Fattoyev, S. Postnikov, and C. J. Horowitz, Phys. Rev. C **93**, 055801 (2016), 1509.06671.